NJC

Accepted Manuscript

This is an *Accepted Manuscript*, which has been through the Royal Society of Chemistry peer review process and has been accepted for publication.

Accepted Manuscripts are published online shortly after acceptance, before technical editing, formatting and proof reading. Using this free service, authors can make their results available to the community, in citable form, before we publish the edited article. We will replace this *Accepted Manuscript* with the edited and formatted *Advance Article* as soon as it is available.

You can find more information about *Accepted Manuscripts* in the Information for Authors.

Please note that technical editing may introduce minor changes to the text and/or graphics, which may alter content. The journal's standard Terms & Conditions and the Ethical guidelines still apply. In no event shall the Royal Society of Chemistry be held responsible for any errors or omissions in this *Accepted Manuscript* or any consequences arising from the use of any information it contains.

ROYAL SOCIETY OF CHEMISTRY

www.rsc.org/njc

Effect of Configurational Isomerism and Polymorphism on Chalcone Fluorescent Properties

Ruimin Zhang, † Mingliang Wang†*, † Hao Sun, †Arshad Khan, † Rabia Usman, † Shengzhi Wang, † Xiantao Gu, † Jia Wang and Chunxiang Xu ‡*

† School of Chemistry and Chemical Engineering, Southeast University, Nanjing 211189, P. R. China

‡ State Key Laboratory of Bioelectronics, Southeast University, Nanjing 210096, P. R. China

*Corresponding author. Tel.: +862585092237. E-mail address: (M.W.) wangmlchem@seu.edu.cn; (C.X.) xcxseu@seu.edu.cn

ABSTRACT. Three chalcones, 3-(9-anthryl)-1-(4-methoxyphenyl)prop-2-en-1-one (**I**), 3-(9-anthryl)-1-phenyl-prop-2-en-1-one (**II**) and 3-(1-pyrenyl)-1-(4-methoxyphenyl)prop-2-en-1-one (**III**), were synthesized and crystallized in different solvents to provide different forms, such as two forms of **I** (**I_a**, **I_b**), four forms of **II** (**II_a**, **II_b**, **II_c**, **II_d**) and four forms of **III** (**III_a**, **III_b**, **III_c**, **III_d**). The single crystal X-ray diffraction were determined except for **II_a**, **III_a**, and **III_c**, powder X-ray diffraction, thermal behaviors, solid-state absorption and fluorescence spectroscopy were investigated for all these crystals. It was found that these forms possess different configurational isomers and conformational polymorphs. Among them **I_a**, **II_d**, **III_b** and **III_d** own trans configuration, while **I_b** and **II_b**, **II_c** show cis configuration with higher melting point than their trans isomers. These forms with trans configuration are fluorescent that **III_b** exists a new red shifted fluorescent peak relative to **III_d** which can be explained by strong slipped face-to-face π-stacked arrangement of pyrene chromophores in **III_b**. **II_d** shows a new red shifted fluorescent peak relative to **I_a** which can be explained by overwhelming C(anthracene)-H…π(anthracene ring) interaction with edge-to-face slipped π-stacked arrangement in **II_d**. Although no single crystal of **II_a**, it can still be speculated that **II_a** owns trans conformation and has stronger interactions of anthracene fluorophores than **II_d** by combining two facts that **II_a** can be formed from **II_d** by heating which is tested by DSC and HSM and exists only a new red shifted fluorescent peak relative to **I_a** or **II_d**.

INTRODUCTION

Crystal polymorphism[1] is a complex phenomenon and seizes the attention of a large number of chemists and crystal engineers because of significantly different physical or chemical properties and potential applications in the manufacture of drugs, explosives, dyes and pigments, and etc.[2] Moreover, polymorphs are valuable for understanding the relationship of crystal packing and structure property.[3] For example, polymorphs have been used for improving some important thermodynamic properties such as solubility and kinetic properties such as dissolution rate and stability, as well as mechanical properties crucial to medicine.[4] Recently, polymorphs have also been used for the development of tuning solid-state luminescence without some difficult chemical reactions.[5]

Chalcones, the chromophoric groups separated by a keto-vinyl chain[6] exhibit many interesting properties such as non-liner optical,[7] fluorescence[8] and biological activities.[9] Many crystal structures of chalcones have been reported in which cis configuration is rarely reported because of obvious steric hindrance.[10] In cis-trans configuration isomer system, symmetric arrangement for atoms makes molecules pack in crystal structure regularly that trans configuration shows more stable structure than cis which was also proved by quantum chemistry method.[11] Yoann Leydet and colleagues detected cis-trans photoisomerization in aqueous solutions for chemical reactions, as well as photochromism between the chalcone-type species.[12] In addition, there are also some reports about the presence of keto-enol tautomeric transition in solution for chalcones.[13] However, no any report about polymorphism of chalcones or effects to properties has been found. In this report, we focus our study on polymorphism of chalcones, especially effects of crystal packing mode on fluorescent properties.

EXPERIMENTAL SECTION

Crystal preparation.

These three compounds 3-(9-anthryl)-1-(4-methoxyphenyl)prop-2-en-1-one (**I**), 3-(9-anthryl)-1- phenyl-prop-2-en-1-one (**II**) and 3-(1-pyrenyl)-1-(4-methoxyphenyl)prop-2-en-1-one (**III**) (Scheme 1) were synthesized according to previously published procedure in our laboratory.[5, 14] Analytical grade solvents were used.

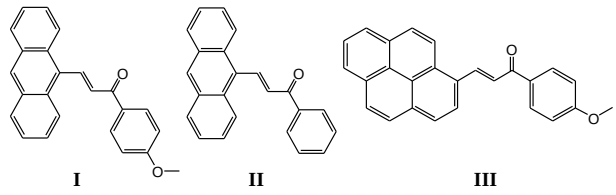

Scheme 1. Chemical structure of **I**, **II**, **III**.

$\mathbf{I_a}$ was recrystallized in ethyl acetate as yellow rodlike crystal. $\mathbf{I_b}$ was got from acetone/acetonitrile (v:v=1:1) mixed solvents in which $\mathbf{I_a}$ was dissolved. Slow evaporation of the solvents at room temperature for 3-4 days yielded light yellow plate (figure S1 of ESI).

$\mathbf{II_a}$ was recrystallized in ethyl acetate(EA)/acetic acid (v:v=1:1) mixed solvents as yellow needlelike crystal. $\mathbf{II_b}$ and $\mathbf{II_c}$ were yielded from acetone/acetonitrile and ethonal/chloroform (v:v=1:1) mixed solvents respectively in which $\mathbf{II_a}$ was dissolved. Slow evaporation of the solvents at room temperature for 4-5 days yielded orange and yellow rodlike crystal, respectively. $\mathbf{II_d}$ was yielded from ethanol solution of $\mathbf{II_a}$. One day later yielded yellow rodlike crystal.

$\mathbf{III_b}$ was recrystallized in acetone/acetonitrile (v:v=1:1) as orange rhombohedral crystal. $\mathbf{III_a}$, $\mathbf{III_c}$ and $\mathbf{III_d}$ were yielded from dichloromethane(DCM)/acetonitrile, ethanol/acetone and dichloromethane/acetone (v:v=1:1) mixed solvents respectively in which $\mathbf{III_b}$ was dissolved. Yellow

rodlike crystal, yellow non-transparent crystal, orange rodlike crystal were got respectively by slow evaporation of the solvents at room temperature for 3-4 days.

Characterization studies

X-ray Diffraction. The powder X-ray diffraction (PXRD) patterns for the ten crystals were recorded using a 18 KW advance X-ray diff ractometer with Cu K α radiation (λ=1.54056 Å). Single crystal X-ray diffraction (SCXRD) data were collected on Nonius CAD4 diffractometer with Mo Kα radiation (λ=0.71073 Å). The structures were solved with direct methods using the SHELXL-2014/7 program and refined anisotropically using full-matrix least-squares procedure.

Spectroscopic Measurements. Fluorescence spectra were obtained on a Horiba FluoroMax 4 spectrofluorometer. UV-Vis absorption spectra were recorded on a Shimadzu UV-3600 spectrometer and the solution state UV-Vis measurements were carried out in 1.0×10^{-6} mol·L^{-1} acetonitrile solution. Infrared spectra were collected on a Bruker Tensor 27 FT-IR spectrometer.

Fluorescence microscopy images. Fluorescence microscopy images were obtained on an Olympus BX51 imaging system excited at 365 nm.

Thermogravimetric Analysis (TGA) and Differential Scanning Calorimetry (DSC). TGA/DSC patterns were recorded with a Mettler-Toledo TGA/DSC Thermogravimetric Analyzer with the temperature scanned from 50 to 400 ℃ at 10 ℃ /min under a dry nitrogen purge (20 mL/min).

Hot stage microscopy(HSM). Hot stage microscopy was performed on a LEICA DM750P microscope using a Mettler-Toledo FP82HT hot stage. The data were visualized using the AMC Capture software.

Results and discussion

Crystal structure

Despite considerable experimental endeavor, attempts to grow single crystals of **II_a**, **III_a** and **III_c** for structure analysis were unsuccessful. Thus, single crystal X-ray diffraction (SCXRD) analysis were performed for other forms showing independent framework arrangements and cell parameters (Table 1). Additionally SCXRD of **I_b** and **II_c** were reported.[15]

Table 1. Crystal data and structure refinement.

crystal	**I_a**	**I_b**[15a]	**II_b**	**II_c**[15b]	**II_d**	**III_b**	**III_d**
Formula	$C_{24}H_{18}O_2$	$C_{24}H_{18}O_2$	$C_{23}H_{16}O$	$C_{23}H_{16}O$	$C_{23}H_{16}O$	$C_{26}H_{18}O_2$	$C_{26}H_{18}O_2$
Temperature/K	293	293	293		293	293	293
Solvent system[a]	EA	acetone/ acetonitrile	acetone/ acetonitrile	ethonal/ chloroform	ethanol	acetone / acetonitrile	DCM/ acetone
Crystal size/mm^3	0.10x0.20 x0.30	0.09x0.27x 0.54	0.10x0.20x 0.30		0.10x0.20x 0.30	0.10x0.20x 0.30	0.10x0.20x 0.30
morphology	plate	rodlike	rodlike	rodlike	rodlike	particle	rodlike
Melting point /℃	139	167	149	147	120,125	154	150
Configuration	trans	cis	cis	cis	trans	trans	trans
Crystal system	Orthorhombic	Monoclinic	Monoclinic	Orthorhombic	Monoclinic	Monoclinic	Monoclinic
Space group	$P2_12_12_1$	Cc	$P2_1/n$	$P2_12_12_1$	$C2/c$	$P2_1/c$	$C2/c$
a/ Å	10.669(2)	5.5018(2)	16.727(3)	14.992(3)	27.135(5)	11.343(2)	29.981(6)
b/ Å	11.771(2)	19.9215(8)	5.6410(11)	19.124(4)	5.8300(12)	7.9890(16)	5.7400(11)
c/ Å	14.278(3)	16.0500(7)	18.544(4)	5.6140(10)	20.776(4)	21.559(4)	21.533(4)
α/deg	90	90	90	90	90	90	90
β/deg	90	95.072(2)	109.35(3)	90	98.03(3)	104.06(3)	91.25(3)
γ/deg	90	90	90	90	90	90	90
V/ Å3	1793.1(6)	1752.26(12)	1650.9(6)	1609.6(6)	3254.5(12)	1895.1(7)	3704.8(13)
Z	4	4	4	4	8	4	8
ρ (calcd)/ Mg m-3	1.2535(4)	1.283	1.241	1.273	1.259	1.270	1.299
θ Range for data collection/ °	2.242-25.363	2.0-26.0	1.423-25.387		1.516-25.425	1.851-25.370	1.359-25.371
F(000)	712	712	648	648	1296	760	1520
R1, w R2 (I > 2σ(I))	0.0580, 0.1496	0.0367, 0.0836	0.0675, 0.1412		0.0698, 0.1151	0.0578, 0.1387	0.0871, 0.1647
R1, w R2 (all data)	0.1189, 0.1862	0.0431, 0.0872	0.1635, 0.1823		0.1709, 0.1422	0.1264, 0.1686	0.1849, 0.2040
Goodness-of-fit	1.002	1.070	1.002		1.001	1.002	1.010
CCDC	1063123	754269	1063126		1063127	1063124	1063125

[a] EA/acetic acid, DCM/acetonitrile and ethanol/acetone for form **II_d**, **III_a** and **III_c**, respectively. The volume ratio of mixed solvents above was v:v=1:1.

From the structure information of Figure 1 to figure 7, it is obvious that **I_a**, **II_d**, **III_b** and **III_d** adopt trans configuration while **I_b**, **II_b** and **II_c** adopt cis configuration with respect to the central C=C bond. Thus,

chalcone **I** and **II** exist configurational isomers while $\mathbf{II_b}$, $\mathbf{II_c}$ and $\mathbf{III_b}$, $\mathbf{III_d}$ are conformational polymorphs in solid state. From crystal structure data the dihedral angles between the benzene ring and anthracene ring of forms of **I** and **II** are obviously greater than the dihedral angles between the benzene ring and pyrene ring of forms of **III** which are 76.9(2) °, 69.50(10) °, 84.14(14) °, 59.7(3) °, 76.52(14) °, 42.20(10) ° and 9.40(15) ° for $\mathbf{I_a}$, $\mathbf{I_b}$, $\mathbf{II_b}$, $\mathbf{II_c}$, $\mathbf{II_d}$, $\mathbf{III_b}$ and $\mathbf{III_d}$, respectively (Table 2). Besides, the prop-2-en-1-one (enone) fragment is substantially twisted, as indicated by the C-C-C-O torsion angle. Bond lengths and angles in these forms are normal and comparable with those observed in the related chalcone compounds.[16] In addition, pyrene rings system of $\mathbf{III_b}$ and $\mathbf{III_d}$ show better planarity with a total puckering amplitude of Q=0.050(3) and 0.098(5)Å while the value of anthracene rings system of $\mathbf{I_a}$, $\mathbf{I_b}$, $\mathbf{II_b}$, $\mathbf{II_c}$ and $\mathbf{II_d}$ is orderly 0.219(8), 0.215(3), 0.142(5), 0.122(8), 0.122(4) Å (table S1 of ESI).[17]

Table 2. The dihedral angles between the benzene ring and anthracene ring/pyrene ring, respectively.

crystal	Angles(°)
$\mathbf{I_a}$	76.9(2)
$\mathbf{I_b}$	69.50(10)
$\mathbf{II_b}$	84.14(14)
$\mathbf{II_c}$	59.7(3)
$\mathbf{II_d}$	76.52(14)
$\mathbf{III_b}$	42.2(10)
$\mathbf{III_d}$	9.40(15)

Form $\mathbf{I_a}$ owns orthorhombic system and space group $P2_12_12_1$ while form $\mathbf{I_b}$ has monoclinic system with space group *Cc*. $\mathbf{I_a}$ are connected by weak hydrogen bond (Table 3) (O1 ···H16A distance: 2.46Å; C-O ···H angle: 164 °) and C (benzene)-H…π (10 atoms of anthracene rings) (Table 4) interations on ac plane and stacked by weak hydrogen bond (O1 ···H24A distance: 2.59Å; C-O ···H angle: 134 °) along c axis (Figure 1b). As shown in Figure 2b, $\mathbf{I_b}$ molecules are connected by weak hydrogen bond (O1 ···H24A distance: 2.59Å; C-O ···H angle: 120 °) and C (anthracene)-H…π (benzene ring) on bc

plane. Moreover, **I_b** are stacking by weak hydrogen bond (O1 ···H8A distance: 2.59Å; C-O ···H angle: 147 °) interactions along a axis. The methoxy groups of **I_a** and **I_b** are almost coplanar with their attached benzene ring [C-C-O-C torsion angles = -1.2(8)°and 2.9(3)°].

Table 3. Intermolecular hydrogen bonds parameters.

crystal	interaction	D-H (Å)	H ···A (Å)	D ···A (Å)	∠D-H ···A (°)
I_a	C_{16}-H_{16}…O_1	0.93	2.46	3.363(7)	164
	C_{24}-H_{24A}…O_1	0.96	2.59	3.333(8)	134
I_b	C_8-H_{8A}…O_1	0.93	2.47	3.290(3)	147
	C_{24}-H_{24}…O_1	0.96	2.59	3.176(4)	120
II_b	C_{16}-H_{16A}…O_1	0.93	2.51	3.321(4)	147
II_c	C_{16}-H_{16}…O	1.17(11)	2.57(2)	3.481(9)	133(19)
II_d	C_8-H_8…O	0.93	2.69	3.556	155
III_b	C_{13}-H_{13A}…O_1	0.93	2.47	3.343(4)	157
	C_{26}-H_{26A}…O_1	0.96	2.50	3.470(4)	158
III_d	C_{22}-H_{22A}…O_2	0.93	2.46	3.301(7)	151

Table 4. C-H···π interactions in these forms.

crystal	interaction	distance (Å)[b]	Angle (°) [c]
I_a	C_{19}-H_{19A}…anthracene	2.94	146
I_b	C_9-H_9…anthracene	3.022(1)	157
	C_{17}-H_{17A}…benzene ring	2.89	145
II_b	C_7-H_7…anthracene rings	3.072	146
	C_9-H_9…anthracene rings	2.984	144
	C_{15}-H_{15A}…anthracene rings	2.970	166
II_c	C_{11}-H_{11}…benzene ring	2.707	151
	C_{15}-H_{15}…anthracene rings	2.687	149
	C_{21}-H_{21}…anthracene rings	3.022	152
II_d	C_{14}-H_{14}…benzene ring	2.892(7)	162
	C_{15}-H_{15}…6 atoms of anthracene ring	3.032(8)	145
	C_{17}-H_{17}…6 atoms of anthracene ring	2.985(9)	142
	C_{19}-H_{19}…6 atoms of anthracene ring	2.856(9)	137
III_b	C_{24}-H_{24}…pyrene rings	2.959(5)	137
	C_{25}-H_{25}…pyrene rings	2.938(6)	143
III_d	C_{16}-H_{16A}…benzene ring	2.648(6)	147

[b]The distances were measured from hydrogen atom to the centre of the aromatic ring (for C-H···π); [c] The angles were measured between C-H-*c*(for C-H···π).

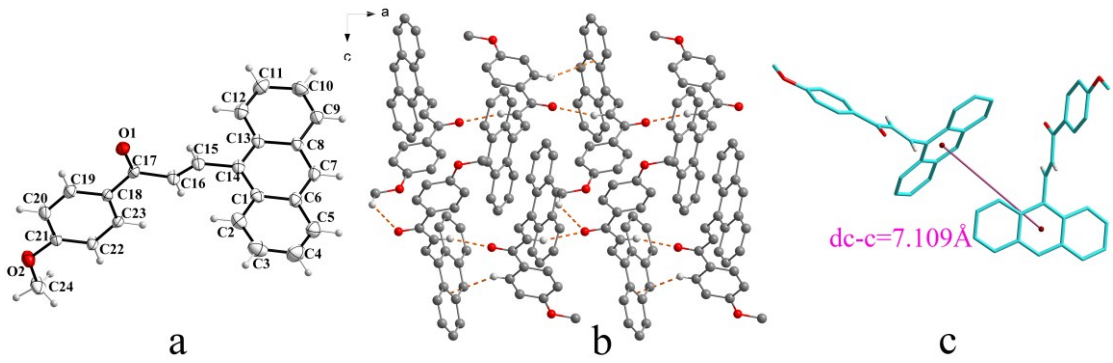

Figure 1. Structure of form $\mathbf{I_a}$: (a) trans configuration, (b) form $\mathbf{I_a}$ molecules are linked by hydrogen bonds and C-H···π interactions on ac plane, (c) The plum line represents the closest centroid distance ($d_{c\text{-}c}$=7.1089Å) between the adjacent anthracene rings. The dotted lines show hydrogen bonds and C-H···π interactions, respectively. Hydrogen atoms not participating in the interactions have been omitted for clarity.

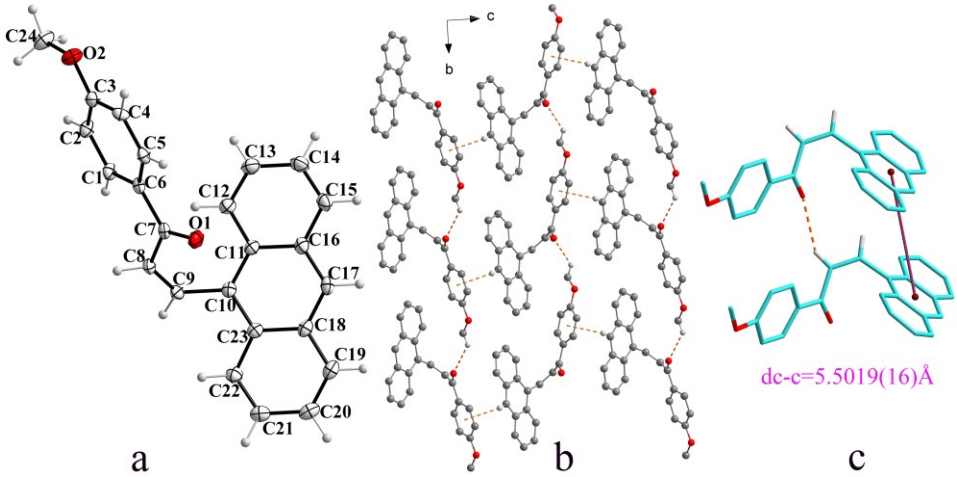

Figure 2. Structure of form $\mathbf{I_b}$: (a) cis configuration, (b) $\mathbf{I_b}$ molecules are linked by hydrogen bonds along b axis and C-H···π interactions along c axis, (c) molecules are stacking along a axis with hydrogen bond. The dotted lines show hydrogen bonds and C-H···π interactions.

The form $\mathbf{II_b}$ crystallizes in monoclinic system with space group $P2_1/n$ and $\mathbf{II_c}$ possesses orthorhombic system and space group of $P2_12_12_1$ whereas the form $\mathbf{II_d}$ crystallizes in monoclinic system with space group $C2/c$. As shown in Figure 3b-5b, these three forms ($\mathbf{II_{b\text{-}d}}$) have different types of C-H…π

interactions that C (benzene)-H…π (benzene) interactions on ac plane in form **II_b**, C (benzene)-H…π (anthracene) and C (anthracene)-H…π (benzene) interactions on ab plane in **II_c** and C (anthracene)-H…π (benzene) interactions on ac plane for form **II_d**.

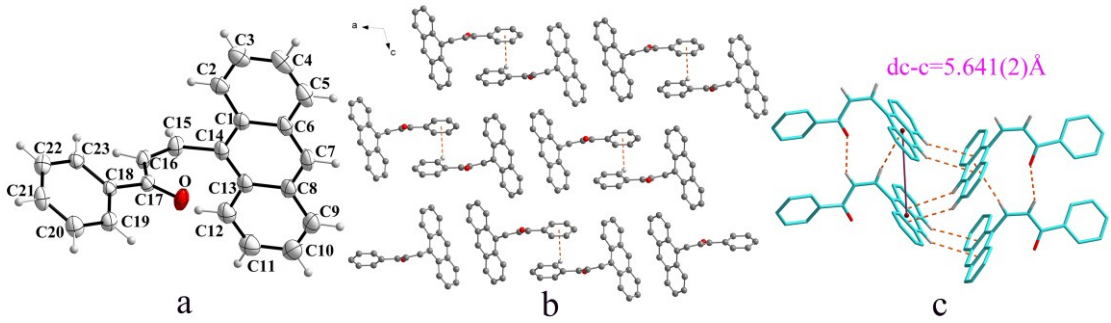

Figure 3. Structure of form **II_b**: (a) cis configuration, (b) **II_b** molecules are linked by C-H···π interactions on ac plane, (c) molecules are stacking along b axis with hydrogen bond and C-H···π interaction with edge-to-face arrangement. The dotted lines show hydrogen bonds and C-H···π interactions.

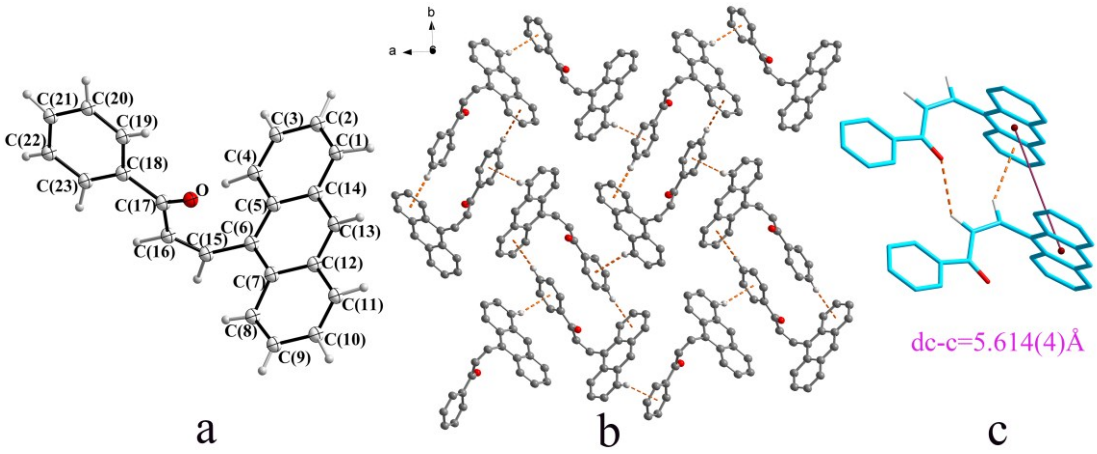

Figure 4. Structure of form **II_c**: (a) cis configuration, (b) **II_c** molecules are linked by C-H···π interactions on ab plane, (c) molecules are stacking along c axis with hydrogen bond. The dotted lines show hydrogen bonds and C-H···π interactions.

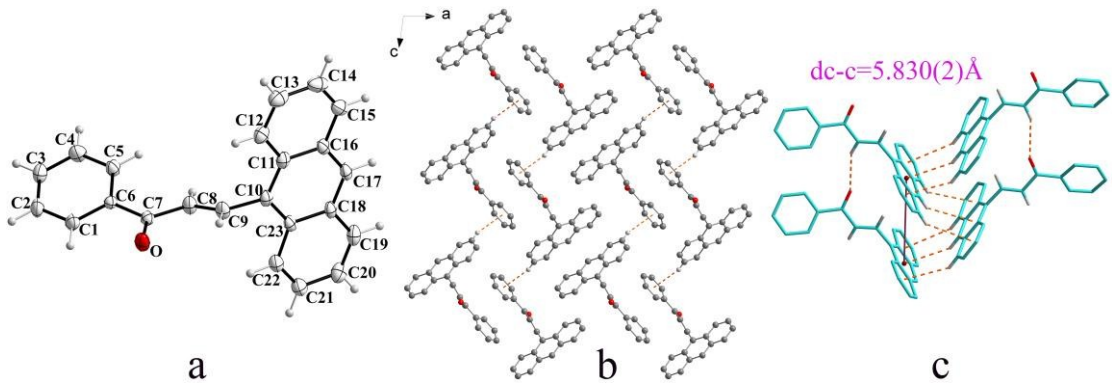

Figure 5. Structure of form $\mathbf{II_d}$: (a)trans configuration, (b) $\mathbf{II_d}$ molecules are linked by C-H···π interactions on ac plane, (c) molecules are stacking along b axis with hydrogen bond and C-H···π interaction with edge-to-face arrangement. The dotted lines show hydrogen bonds and C-H ··π interactions.

$\mathbf{III_b}$ forms in monoclinic system with space group $P2_1/c$ while $\mathbf{III_d}$ crystallizes in monoclinic system with $C2/c$. As shown in figure 6 and 7, both of $\mathbf{III_b}$ and $\mathbf{III_d}$ exist in trans configuration with similar crystal structure that pyrene rings with two directions are parallel stacking along b axis. In $\mathbf{III_b}$, there exist C (benzene)-H…π (pyrene) and weak hydrogen bond (O1 ··H26A distance: 2.50Å; C-O ··H angle: 158°) on ac plane forming a big ring. $\mathbf{III_d}$ molecules are connected by C(pyrene)-H…π(benzene) interactions and hydrogen bond (O2 ··H22A distance: 2.46Å; C-O ··H angle: 151°) on ac plane. The methoxy groups of $\mathbf{III_b}$ and $\mathbf{III_d}$ lie in the plane of the benzene ring to which it is connected [C-C-O-C torsion angles = -6.7(4)°and -2.3(6)°].

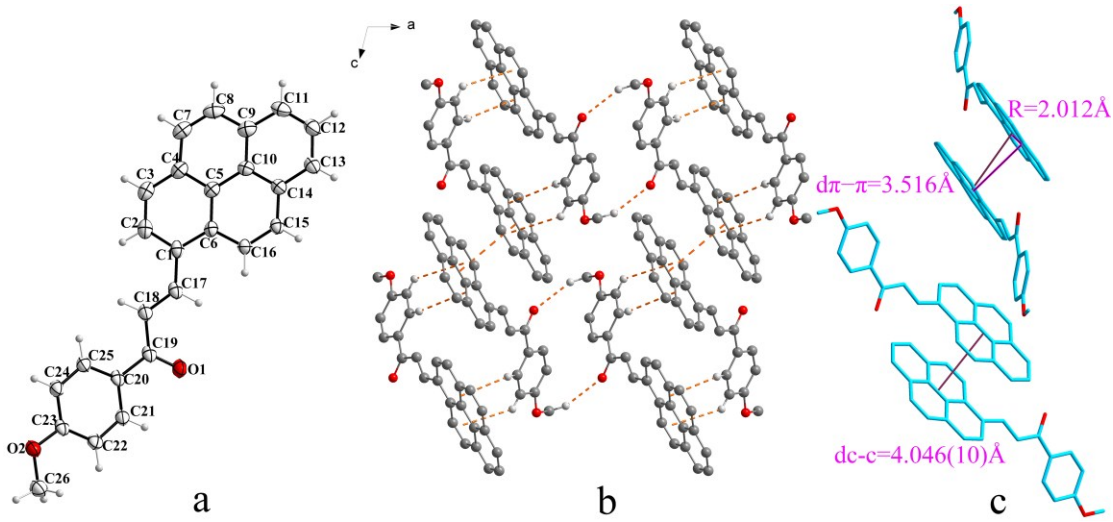

Figure 6. Structure of form $\mathbf{III_b}$: (a) trans configuration, (b) $\mathbf{III_b}$ molecules are linked by hydrogen bonds and C-H···π interactions on ac plane, (c) molecules are stacking along b axis with face-to-face slipped π···π interaction forming inverse dimers. The dc-c, dπ−π and R are 4.046(10)Å, 3.516Å and 2.012Å, respectively. The dotted lines show hydrogen bonds and C-H···π interactions, respectively.

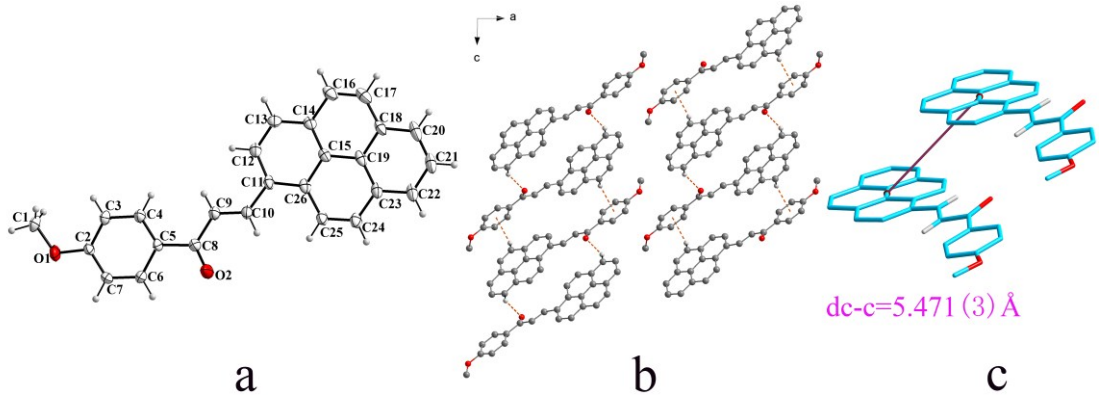

Figure 7. Structure of form $\mathbf{III_d}$: (a) trans configuration, (b) $\mathbf{III_d}$ molecules are linked by hydrogen bonds and C-H···π interactions on ac plane, (c) molecules show no interactions along b axis. The dotted lines show hydrogen bonds and C-H···π interactions, respectively.

Above all, except for mononer arrangement of $\mathbf{I_a}$, all other forms adopt parallel face-to-face slipped stacked arrangement for anthracene or pyrene rings. As shown in table 5, the closest centroid distance

(d_{c-c}) between adjacent anthracene rings are 7.109Å, 5.5019(16)Å, 5.641(2)Å, 5.614(4)Å and 5.830(2)Å for **I_a**, **I_b**, **II_b**, **II_c** and **II_d** and the closest d_{c-c} between pyrene rings is 5.471(3)Å for **III_d** respectively, which indicates there is no effective π...π interactions between chromophores in these forms.[18] Dramatically, the closest centroid distance (d_{c-c}) between pyrene rings in **III_b** is 4.046(10)Å and the interplanar separation ($d_{\pi-\pi}$) and lateral displacement (R)[15] between the mean planes of the pyrene moieties are 3.516Å and 2.012Å respectively, which implies π-π interactions existing between the neighboring pyrene chromophores. As shown in Figue 6(c), pyrene planes in **III_b** adopt face-to-face stacked arrangement and form inverted dimers. Moreover, it is obvious that anthracene moieties of **II_b** and **II_d** adopt edge-to-face arrangement stacked with C(anthracene)-H…π (anthracene) interactions shown in Figure 3c and 5c. In addition, all of **I_b**, **II_b**, **II_c** and **II_d** are linked by C(alkene)-H…O(carbonyl) interactions along stacking orientation.

Table 5. The closest centroid distance dc-c between anthracene or pyrene rings.

crystal	d_{c-c}(Å)
I_a	7.109
I_b	5.5019(16)
II_b	5.641(2)
II_c	5.614(4)
II_d	5.830(2)
III_b	4.406(10)
III_d	5.471(3)

Powder X-ray Diffraction analysis

All these crystals were determined by powder X-ray diffraction analysis. Remarkably, the PXRD patterns indicate distinct difference and provide unambiguous proofs for isomers and polymorphs (figure 8). Furthermore, PXRD curves coincide well with simulated XRD patterns indicating these forms with high purity (figure S2 of ESI). However, the PXRD patterns have deviations in diffraction

intensity relative to their simulated patterns, which presumably correlates with the morphology of the samples grinded for PXRD analysis.

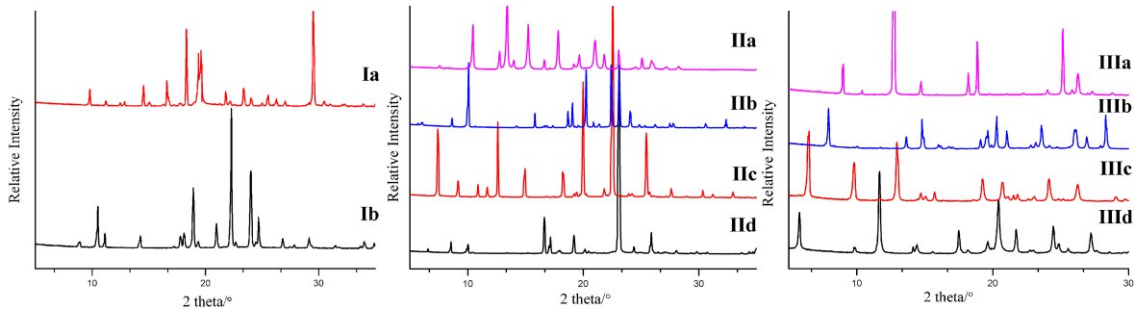

Figure 8. PXRD patterns of crystals.

Thermal properties and polymorph transition

The thermal behaviors of these crystals were investigated by DSC and TGA. As shown in figure 9, $\mathbf{I_a}$ exhibits one lower endothermic peak at 139 ℃ than $\mathbf{I_b}$ at 167 ℃. Similarly, $\mathbf{II_a}$, $\mathbf{II_b}$ and $\mathbf{II_c}$ exist one endothermic peak at 125 ℃, 149 ℃ and 147 ℃ respectively while $\mathbf{II_d}$ has two close endothermic peaks at 120 ℃ and 125 ℃. $\mathbf{III_a}$, $\mathbf{III_b}$, $\mathbf{III_c}$ and $\mathbf{III_d}$ have one endothermic peak at 147 ℃, 154 ℃, 162 ℃ and 150 ℃, respectively. It is noted that those forms with fluorescence nearly show lower melting point than forms without fluorescence (table S2 of ESI).

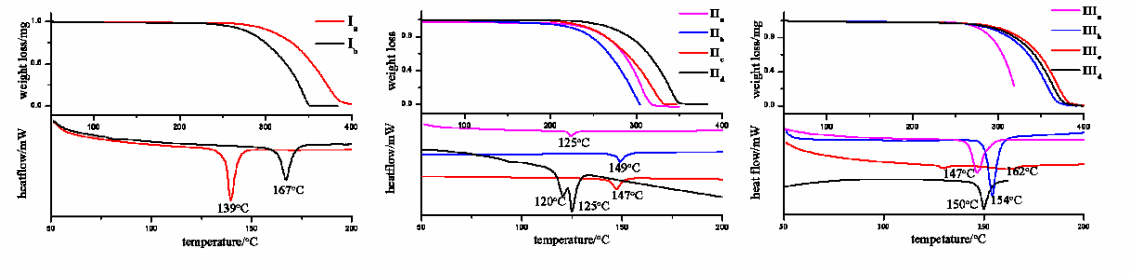

Figure 9. TGA/DSC profiles of crystals.

Because of the same endothermic peak for $\mathbf{II_a}$ and $\mathbf{II_d}$ at 125 ℃, hot-stage microscopy (HSM) experiments were performed to explore the relationship between these two forms in the process of

melting at 1 ℃/min. It can be seen from Figure 10 that crystal of **II$_d$** began to melt at 102 ℃ and new needle crystal (**II$_{d-x}$**) generated from the liquid phase at 113 ℃, which is a melting and recrystallization process. With the temperature increasing, more needle crystals could be observed rapidly and then all the needle crystals began to melt at 120-122 ℃ again, which is consistent with **II$_a$**, suggesting the same phase with form **II$_a$** generating during the heating process. In addition, there should be another form of **II$_a$** which is less stable form melting at 120 ℃ on second heating of **II$_a$** (Figure S3 of ESI).

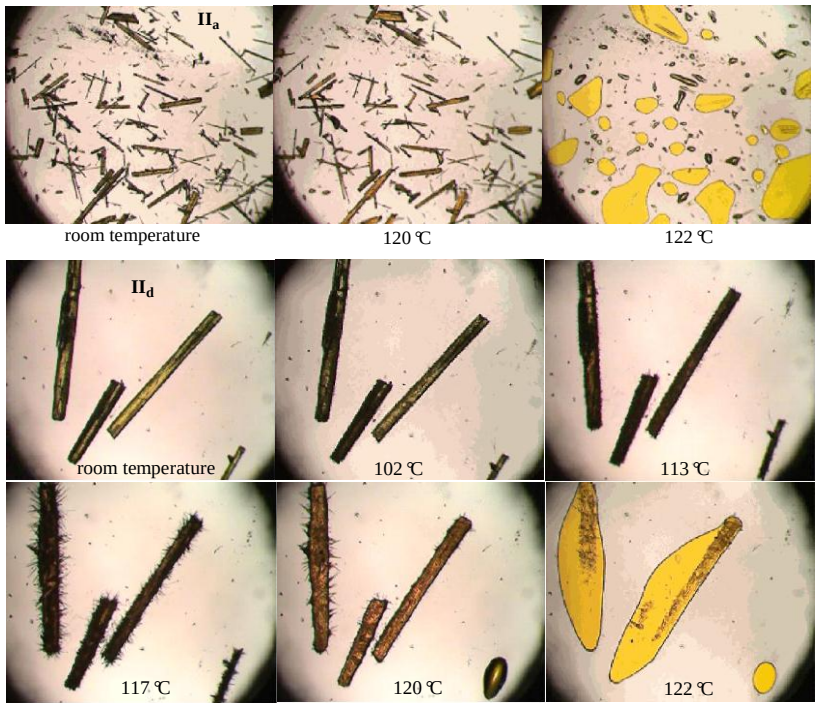

Figure 10. Photomicrographs of form **II$_a$** and **II$_d$** at various temperatures in the HSM experiment. Notice that needle crystals (**II$_{d-x}$**) generated from the liquid phase of **II$_d$**.

More importantly, it is noted that **II$_{d-x}$** and **II$_a$** are identical forms by comparing their PXRD patterns (Figure 11)[19]. Hence, it provides evidence that form **II$_d$** is in metastable state and it can transform into form **II$_a$** by heating. Thus, there is a deduction that form **II$_a$** owns trans configuration. The same experiments were measured for other forms without polymorph transition.

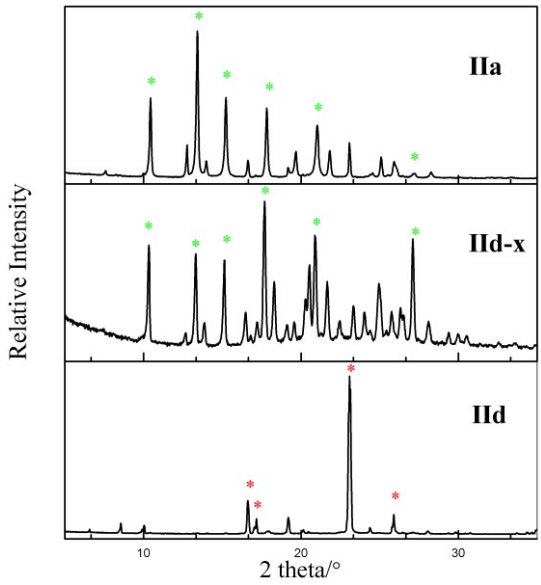

Figure 11. Comparison of PXRD patterns of new needle crystals ($\mathbf{II_{d\text{-}x}}$) obtained after heating of $\mathbf{II_d}$ with $\mathbf{II_a}$. (* stand for the same prominent peaks for form $\mathbf{II_a}$ and $\mathbf{II_{d\text{-}x}}$ and * are for form $\mathbf{II_d}$)

Optical-Physical Properties.

FT-IR Spectroscopy, diffuse reflectance absorption spectroscopy and fluorescence emission spectroscopy were performed to investigate the non-covalent interactions and optical properties of these crystals.

From FT-IR spectra (figure S4 of ESI), two strong vibrational absorption peaks in 1670-1590 cm^{-1} range magnified in the figure should be assigned to the carbonyl group with high frequency and ethenyl group of every form, respectively. All forms of **I** and **II** in acetonitrile have similar absorption spectra with three peaks between 300-400nm which are ascribed to anthracene.[20] All polymorphs of **III** in acetonitrile have also similar absorption spectra with two peak between 270-450nm arising from pyrene (Figure S5 of ESI).[14] The diffuse reflectance spectra of all crystals show a broad band located at

350-500nm and 400-700nm (Figure 12) which indicates obvious red shift relative to the absorption in solution by molecular aggregates.[21]

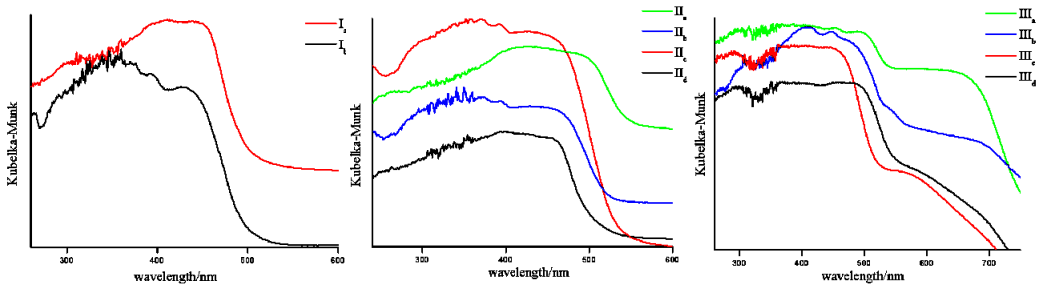

Figure 12. Solid-state adsorption spectra of crystals.

Fluorescence spectra (λex=365 nm) in cyclohexane solution (Figure S6 of ESI) and solid-state emission spectroscopy were also exploited for all those forms (Figure 13 and table S3 of ESI). Remarkably, it was found that only those with trans configuration are fluorescent in solid-state. **I_a** shows one peak at 495nm ascribed to emission of anthracene moiety whereas **II_d** shows a new red shifted fluorescent peak at 526nm relative to **I_a** which can be explained by overwhelming C(anthracene)-H…π (anthracene) interactions with edge-to-face slipped π-stacked arrangement for anthracene moieties. As two facts that **II_a** can be formed from **II_d** by heating which is tested by DSC and HSM and **II_a** exists only the new red shifted fluorescent peak at 545nm compared to **I_a** or **II_d**, it can be speculated that **II_a** own trans configuration and adopts stronger interactions between anthracene fluorophores than **II_d.** Similarly, **III_d** shows one peak at 583nm which can be ascribed to emission from pyrene. **III_b** exists a new red shifted fluorescent peak at 603nm relative to **III_d** which could be ascribed to stronger slipped face-to-face π-stacked arrangement of pyrene fluorophores in **III_b**.

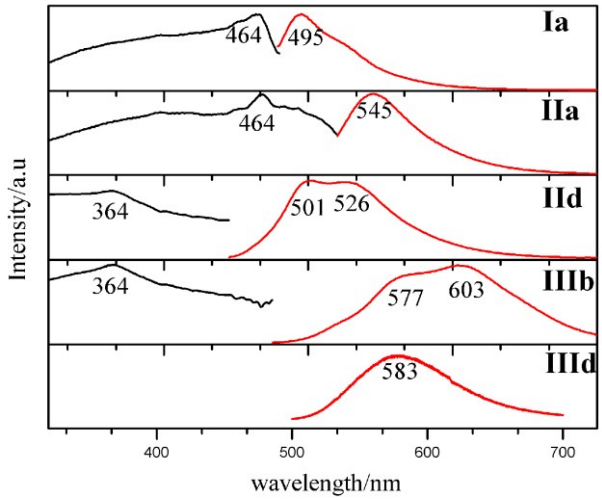

Figure 13. Solid-state excitation spectra (black) and fluorescence emission spectra (red).

Fluorescence microscopy images by irradiating the crystals with UV light (Figure 14) reveal different fluorescence colors of these forms and coincide with their emission spectrum, which can be clearly detected visually. All these results clearly demonstrate that the optical-physical properties of the crystals are dependent on the intermolecular interactions and packing mode of fluorophores in solid state.

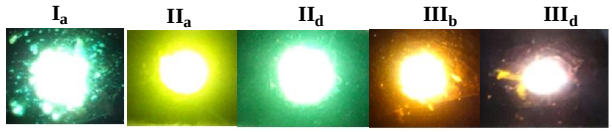

Figure 14. Fluorescence microscopy images of three crystals under UV light (λex=365 nm).

CONCLUSION

In summary, we have successfully prepared different chalcones by solution method. Crystal structures reveal that $\mathbf{I_a}$, $\mathbf{II_d}$, $\mathbf{III_b}$ and $\mathbf{III_d}$ own trans configuration while $\mathbf{I_b}$ and $\mathbf{II_b}$, $\mathbf{II_c}$ own cis configuration. In comparison with cis-isomer, the trans-configuration is beneficial to the solid fluorescence. Moreover, the arrangements of anthracene or pyrene chromophores in these forms could be classified into three types: monomer arrangement (form $\mathbf{I_a}$, $\mathbf{I_b}$, $\mathbf{II_c}$ and $\mathbf{III_d}$), edge-to-face π-π stacking (form $\mathbf{II_b}$ and $\mathbf{II_d}$),

and face-to-face π-π stacking (form **III_b**). The π-stacked geometries of anthracene or pyrene fluorophores are responsible for the larger red-shifted emissions in **II_b**, **II_d** and **III_b**. Although no single crystal data of **II_a**, it can still be speculated that **II_a** own trans configuration and adopt stronger interactions between anthracene fluorophores than **II_d** by combining two facts that **II_a** can be formed from **II_d** by heating which is tested by DSC and HSM and **II_a** exists only the new red shifted fluorescent peak compared to **I_a** or **II_d**. The discovery based on the configurational isomerism and polymorphism of chalcones, especially effects of crystal packing mode on fluorescent properties could provide profound significance for organic light-emitting materials.

ACKNOWLEDGMENT

This project gets the supports of the National Basic Research Program of China (2011CB302004).

REFERENCES

1. J. P. Brog**,** C. L. Chanez**,** A Crochet and K. M. Fromm**,** *RSC Adv.*, 2013, **3**, 16905-16931.
2. (a) R. D. Gautam, *Cryst. Growth Des*., 2008, **8,** 1-3; (b) J. Elguero, *Cryst. Growth Des*., 2011, **11,** 4731-4738.
3. J. Bernstein, *Polymorphism in Molecular Crystals*; Oxford University Press: New York, 2002.
4. B. J. Venhuis, M. V. Vredenbregt, N. Kaun, J. K. Maurin and Z. Fijalek, *J. Pharm. Biomed. Anal*,. 2011, **54**(1), 21-26.
5. Q. Feng, M. L. Wang, B. L. Dong, C. X. Xu, J. Zhao and H. J. Zhang, *CrystEngComm.,* 2013, **15**, 3623-3629.
6. (a) M. L. Go, X. Wu and L. X. Liu, *Curr. Med. Chem.*, 2005, **12**, 483-499; (b) C. N. Khobragade, R. G. Bodage and M. S. Shine, *Enzym. Inhib. Med. Chem.*, 2008, **3**, 341-346.
7. (a) A. Kumar, V. Deval and P. Tandon, *Spectrochim. Acta, Part A*, 2014, **130**, 41-53; (b) Y. F. Sun, H. P. Wang and Z. Y. Chen, *J. Fluoresc.*, 2013, **23**, 123-130; (c) S. Sumathi, P. Tharmaraj and C. D. Sheela, *J. Coor. Chem.,* 2011, **64**(10), 1707-1717; (d) H. J. Ravindra, A. john kiran, K. Chandrasekharan, H. D. Shashikala and S. M. Dharmaprakash, *Appl. Phys.* B, 2007, **88**, 105-110; (e) H. K. Fun, R. Kia, P. S. Patil, S. M.Dharmaprakash and I. A. Razak, *Acta Crystallogr., Sect E,*

2008, **64**, o2014-o2015; (f) P. S. Patil, S. M. Dharmaprakash, K. Ramakrishna, H. K. Fun, R. S. S. Kumar and D. Narayana Rao, *J. Cryst. Growth.*, 2007, **303**, 520-524.

8. (a) T. Kobkeatthawin, S. Chantrapromma, N. Saewanand and H. K. Fun, *Acta Crystallogr., Sect E,* 2011, **67**, o1204-o1205; (b) M. Gaber, S. A. El-Daly, T. A. Fayed and Y. S. El-Sayed, *J. Opt. Laser Techol.,* 2008, **40**, 528-537; (c) S. Chantrapromma, T. Kobkeatthawin, K. Chanawanno, P. Wisitsak and H. K. Fun, *Acta Crystallogr., Sect E,* 2011, **67**, o1770-o1771; (d) F. J. Huo, J. Kang, C. X. Yin, J. B. Chao and Y. B. Zhang, *Sens. Actuators, B,* 2015, **215**, 93-98.

9. (a) S. Mishra, V. Tirkey and A. Ghosh, *J. Mol. Struct.*, 2015, **1085**, 162–172. (b) W. A. Silva, C. C. Gatto and G. R. Oliveira, *Acta Crystallogr., Sect E,* 2011, **67**, o2210; (c) H. K. Fun, C. S. Yeap, D. J. Prasad, S. P. Nayak and K. Laxmana, *Acta Crystallogr., Sect E,* 2011, **67**, o241; (d) L. F. Motta, A. C. Gaudio and Y. Takahata, *J. Mol. Des.*, 2006, **5**(12), 555-569.

10. J. Joothamongkhon, S. Chantrapromma, T. Kobkeatthawin and H. -K. Fun, *Acta Crystallogr., Sect E,* 2010, **66**, o2669-o2670.

11. (a) H. Singh, J. Sindhu and J. M. Khurana, *J. Lumin.*, 2015, **158**, 340–350; (b) R. Nithya, N. Santhanamoorthi, P.Kolandaivel and K. Senthilkumar, *J. Phys. Chem. A,* 2011, **115**, 6594-6602.

12. Y. Leydet, A. J. Parola and F. Pina, *Chem.—Eur. J.*, 2010, **16**, 545-555.

13. (a) I. G. Mamedov, M. R. Bayramov, Y. V. Mamedova and A. M. Maharramov, *Magn. Reson. Chem.*, 2013, **51**, 600-604; (b) I. G. Mamedov, M. R. Bayramov, Y. V. Mamedova and A. M. Maharramov, *Magn. Reson. Chem.*, 2015, **53**, 147-153; (c) M. Wera, A. G. Chalyi, A. D. Roshal, B. Zadykowicz and J. Blazejowski, *Struct. Chem.*, 2014, **25**, 969-977.

14. Q. Feng, M. L. Wang, B. L. Dong, J. He and C. X. Xu, *Cryst. Growth Des.*, 2013, **13**, 4418-4427.

15. (a) Y. Mori and K. Maeda, *Acta Crystallogr., Sect B,* 1994, **50**, 106; (b) S. Chantrapromma, J. Horkaew, T. Suwunwong and H. K. Fun, *Acta Crystallogr., Sect E,* 2009, **65**, o2673-02679.

16. (a) J. P. Jasinski, R. J. Butcher, V. M. Khaleel, B. K. Sarojini and H. S. Yathirajan, *Acta Crystallogr., Sect E,* 2011, **67**, o795; (b) R. Prasath, P. Bhavana and E. R. T. Tiekink, *Acta Crystallogr., Sect E,* 2011, **67**, o796–o797; (c) T. Suwunwong, S. Chantrapromma, C. Karalai, P. Pakdeevanich and H. Fun, *Acta Crystallogr., Sect E,* 2009, **65**, o420–o421; (d) S. Sarveswari, V. Vijayakumar, T. Narasimhamurthy and E. R. T. Tiekink, *Acta Crystallogr., Sect E,* 2010, **66**, o3284; (e) J. Joothamongkhon, S. Chantrapromma, T. Kobkeatthawin and H. Fun, *Acta Crystallogr., Sect E,* 2010, **66**, o2669–o2670.

17. (a) V. T. M. Flores-a and M. A. Iglesias-arteaga, *J Chem Crystallogr.*, 2015, **45**, 14–119; (b) R. Sudheer, M. Sithambaresan, N. R. Sajitha and E. Manoj, *Acta Crystallogr., Sect E,* 2015, **71**, 702–705.

18. C. Janiak, *J. Chem. Soc., Dalton Trans.*, 2000, 3885-3896.

19. X. J. Wu, M. L. Wang, M. Du, J. Lu and J. X. Chen, *Cryst. Growth Des.*, 2015, **15**(1), 434–441.

20. B. L. Dong, M. L. Wang, C. X. Xu, Q. Feng and Y. Wang, *Cryst. Growth Des.*, 2012, **12**(12), 5986-5993.

21. H. B. Rodr ́guez, M. G. Lagorio and E. S. Rom án, *Photochem. Photobiol. Sci.*, 2004, **3**, 674-680.

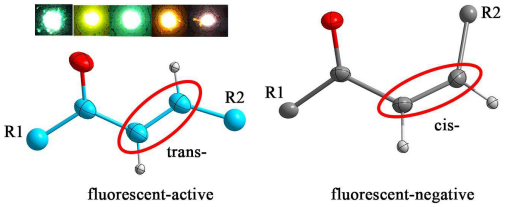

Comparison with cis-isomer, the trans-isomer with different configuration or conformation is beneficial to the solid fluorescence.